Q. J. R. Meteorol. Soc. (2003), **129**, pp. 411–431 doi: 10.1256/qj.02.08

Airflow within major Alpine river valleys under heavy rainfall

By MATTHIAS STEINER[1]*, OLIVIER BOUSQUET[2], ROBERT A. HOUZE JR[2], BRADLEY F. SMULL[2,3] and MARCO MANCINI[4]

[1]*Princeton University, USA*
[2]*University of Washington, Seattle, USA*
[3]*National Severe Storms Laboratory, NOAA, Oklahoma, USA*
[4]*Politecnico di Milano, Italy*

(Received 14 January 2002; revised 7 June 2002)

SUMMARY

This study documents the airflow within major Alpine river valleys in the presence of precipitation. The analysis seeks a conceptual understanding of the effect of rain on the valley flow. Ground-based and airborne Doppler radar and surface data from the Mesoscale Alpine Programme show that during persistent rainy periods the subsidence caused by melting and evaporation of precipitation particles contributes to the formation of a down-valley flow. This down-valley flow opposes moist southerly flow aloft, which is lifted over the topographic barrier and in which precipitation particles are formed.

KEYWORDS: Doppler radar Drainage flow Evaporation Melting Mesoscale Alpine Programme Orographic precipitation Subsidence

1. INTRODUCTION

The flow of air within deep valleys has been extensively studied for dry conditions. Banta and Cotton (1981), Whiteman (1982), Vergeiner and Dreiseitl (1987), Whiteman (1990), Li and Atkinson (1999) and Stewart *et al.* (2002) provided an historical perspective on valley flow research and summarized present understanding of the driving mechanisms. Steinacker (1984) and McKee and O'Neal (1989) elaborated on the role of valley geometry, while Barr and Orgill (1989), Orgill *et al.* (1992) and Whiteman and Doran (1993) detailed the relationship between overlying synoptic flow and winds within a valley. Post and Neff (1986) and Neff (1990) provided insights from a remote-sensing perspective. Desiato *et al.* (1998) and Dosio *et al.* (2001) discussed simulated, dry condition wind fields in major valleys on the south side of the Alps.

By contrast, airflow within valleys under rainfall has received little attention and been studied in much less detail. Orgill *et al.* (1992) mentioned an effect of rain evaporation in orographic flow; however, they did not elaborate. Ohata *et al.* (1981) and Zängl *et al.* (2001), investigating the airflow in high-altitude (>4000 m) valleys of the Himalayas, also suggested an effect of rainfall on the valley flow but were not specific.

Over the years, some studies of rainfall on the windward side of mountain ranges have noted downslope flow during rainy conditions; however, they have not related this downslope flow to conditions within specific river valleys embedded in the larger topographic barrier. Lammert (1920), Frey (1953) and Seibert (1990) described downslope flow under heavy rainfall conditions on the south side of the European Alps. These studies identified a typical situation consisting of a stable stratification south of the Alps, in which air in the lowest levels of the wide Po river basin (often called the Po valley) remains blocked, and only air at approximately 2 km or above rises as it flows northward over the Alpine barrier in association with heavy rainfall on the south side. Such precipitation-related downslope-flow effects, however, are not peculiar to the Alps and have been observed in many places around the world. For example, Marwitz (1980)

* Corresponding author: Department of Civil and Environmental Engineering, Princeton University, Princeton, New Jersey 08544, USA. e-mail: msteiner@princeton.edu

found that during the stable stage of storms over the San Juan Mountains of Colorado much of the flow below mountain-top level is blocked and diverted back downslope. Hill (1978) used a parachute-borne vertical-motion sensor to collect data in orographic clouds over the Wasatch Mountains in Utah. His data suggested that, as precipitation developed, upslope flow reversed to downslope at low levels. Similar effects were also observed near Salt Lake City, Utah (Astling 1984), along the California coastal mountains (Neiman *et al.* 2002), on the trade wind side of the Hawaiian Islands (Carbone *et al.* 1995, 1998), and over the Ghat Mountains (Grossman and Durran 1984).

In this study, we present further and considerably more detailed empirical evidence concerning the occurrence and underlying nature of downslope flow during periods of sustained orographic precipitation. We examine specifically the development of downslope and down-valley flow within narrow river valleys on the windward side of a major mountain barrier. We use data collected in the European Alps as part of the Mesoscale Alpine Programme (MAP) during the autumn of 1999 (Bougeault *et al.* 2001). The Mediterranean side of the Alpine barrier is prone to heavy rainfall and flooding episodes at this time of year (Frei and Schär 1998). Heavy precipitation can be the result of either convective or non-convective processes, or some combination thereof (e.g. Buzzi and Foschini 2000). Generally, these storms occur with the passage of baroclinic waves. Strong low-level southerly flow from the Mediterranean Sea provides the moisture for these precipitation events (Buzzi *et al.* 1998; Doswell *et al.* 1998; Schneidereit and Schär 2000; Rotunno and Ferretti 2001; Houze *et al.* 2001; Gabella and Mantonvani 2001). Often, these heavy and generally stratiform rainfall events may contain embedded convective cells that are triggered by the passage of the low-level flow over topographic features in the lower reaches of the Alpine terrain (Medina and Houze 2003).

The instrumentation deployed during the MAP Special Observing Period (SOP), and relevant to this study, included mobile Doppler radars capable of mapping the flow within individual river valleys. These radars included the ground-based Doppler-on-Wheels (DOW) radar (Wurman *et al.* 1997) and airborne Doppler radars aboard the National Oceanic and Atmospheric Administration (NOAA) P-3 aircraft (Jorgensen *et al.* 1996) and National Center for Atmospheric Research (NCAR) Electra aircraft (Hildebrand *et al.* 1994). Houze *et al.* (2000), Steiner *et al.* (2000) and Smull *et al.* (2000) have shown glimpses of the down-valley flow observed with these instruments. Doppler radar allows for detailed variations of the valley flow to be related directly to the three-dimensional (3D) hydrometeor field.

The purpose of this paper is to use these Doppler radar measurements to document airflow within the valley in relation to fallout, melting, and evaporation of precipitation. We show that during major rain events a significant down-valley flow can develop in the presence of what is broadly regarded as upslope orographic precipitation, describe some of the characteristics of this flow (strength, depth, timing, and coincidence of its top with the melting layer), and offer a physical interpretation. We thereby advance a conceptual understanding of the mechanism of the downslope, down-valley flow as resulting from a dynamic–microphysical feedback process. More specifically, we argue that the down-valley flow is driven in part by melting and evaporation, somewhat analogous to the mesoscale downdraught in the anvil region of a mesoscale convective system (MCS).

2. Geographical setting and data

This study is focused on the Lago Maggiore region, located on the south side of the European Alps near the Swiss–Italian border. Specifically, we have examined data

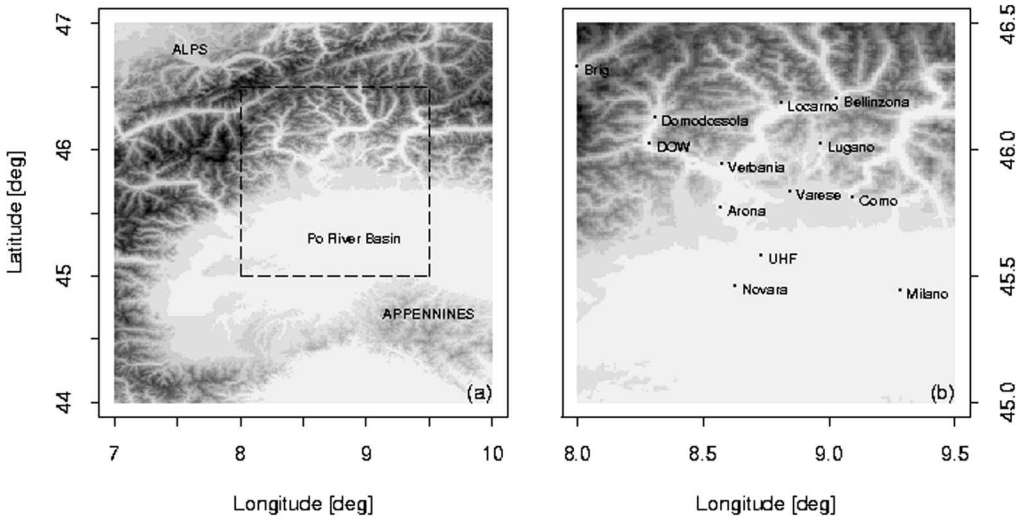

Figure 1. Geographical setting of the Lago Maggiore study area. Shown are the north-western corner of the Po river basin and the surrounding Alpine barrier (the grey scale ranges from 0 to 4000 m) with its major river valleys. The dashed box in the left panel is shown in more detail in the right panel. The Toce river feeds into the Lago Maggiore near Verbania. The L-shaped valley has an approximately east–west oriented lower and a north–south oriented upper part. Domodossola is the largest city in the Toce river valley. The location of the hydrometeorological surface station and the mobile Doppler radar deployment near Pieve Vergonte is marked DOW. The wind profiler location is indicated by UHF.

collected in the Toce river valley (Valle d'Ossola), in north-western Italy, where a concave segment of the Alpine barrier bounds the wide Po river basin (Fig. 1). Data sources include ground-based (DOW) and airborne (dual-beam system aboard the NOAA P-3) mobile X-band scanning Doppler radars, a special surface hydrometeorological station near the DOW deployment site, the 1274 MHz Météo-France ultra high frequency (UHF) wind profiler (Caccia *et al.* 2001) located at Lonate Pozzolo, and serial upper-air soundings launched from the Milano-Linate airport. Figure 1 shows the topography of the region and the location of stations referred to in this paper.

During Intensive Observing Periods (IOPs) of the SOP, the DOW was deployed at either one of two sites in the Ticino river valley (i.e. one near Locarno at the north-east end of the Lago Maggiore and another north of Bellinzona closer to the Alpine crest), or at a third location in the Toce river valley (i.e. south of Domodossola in the prominent bend of this L-shaped valley). The DOW's scanning strategy consisted of one multi-elevation volume scan, followed by several vertical cross-sections aligned up, down, and across the valley. This sequence required about 10–15 minutes and was repeated continuously throughout each storm. The spatial resolution of the data was 1 degree in azimuth and 75 m in radial direction. Further details about the DOW operations and preliminary results can be found in Steiner *et al.* (2000). This study uses data collected at the site near Pieve Vergonte in the Toce river valley (DOW in Fig. 1(b)).

The DOW provided fields of radar reflectivity and radial velocity. Vertical profiles of wind velocity (speed and direction) were retrieved from the radial velocity field by means of the velocity–azimuth display (VAD) technique (Lhermitte and Atlas 1961; Caton 1963; Browning and Wexler 1968), using software developed by Srivastava *et al.* (1986) and Matejka and Srivastava (1991). We limited the VAD analysis to data within a radius of 5 km from the radar.

The DOW deployment site (altitude 225 m*) in the Toce river valley was approximately 200 m from a hydrometeorological station installed by the Politecnico di Milano for the duration of the SOP. Part of the data collected at 30-minute intervals at this surface station has been used in the subsequent analyses. Unfortunately the dew-point temperature (i.e. moisture) measurements were not reliable.

The NOAA P-3 and NCAR Electra research aircraft provided another important source of Doppler radar measurements over and around the Alps during the SOP. Owing to their elevated perspective and extreme mobility, these platforms offered a unique opportunity to probe conditions within multiple deep Alpine valleys, where views from fixed, ground-based radars were blocked by intervening terrain and/or restricted to single-Doppler coverage. Airborne Doppler analyses enable us to link tightly channelled valley flows to large-scale forcing and other processes occurring above and upstream of the mountain barrier. The fixed, ground-based DOW observations, on the other hand, provide temporal continuity not achievable by the airborne platform. For the airborne radar scanning geometry considered here, independent estimates of wind velocity may be reliably synthesized on a Cartesian grid having horizontal and vertical resolutions of 500 and 250 m, respectively. This was done following the variational formalism of Bousquet and Chong (1998) and Georgis *et al.* (2000). Smull *et al.* (2000) provide further details about the data processing. To enable comparison with the DOW profile analyses, the P-3 data were averaged within a 10 km by 10 km domain centred on the DOW location.

The Milano soundings and the Lonate Pozzolo wind profiler provided the closest upper-air data to assess upstream conditions of an approaching air mass and evaluate atmospheric stability. The wind profiler yielded near-continuous coverage of the vertical wind profile; however, only the Milano soundings provided thermodynamic information.

3. Observations in MAP IOP 8

The down-valley flow documented in IOP 8 was by far the most persistent and strongest case encountered during the SOP. Because it was also well covered by ground-based and airborne Doppler radar observations, this case provides an ideal opportunity to examine this striking phenomenon.

Figures 2(a), (b) and (c) show quasi-horizontal and vertical cross-sections of radial Doppler velocity (left-hand panels) and radar reflectivity (right-hand panels) measured by the DOW in the Toce river valley at about 0950 UTC 21 October 1999. The structures shown in these cross-sections are typical of those observed throughout IOP 8. The topography restricted the radar observations at low levels to within the valley (Fig. 2(a)). The DOW, located at the sharp bend of the Toce river valley, observed relatively uniform rainfall and continuous down-valley directed airflow through the sampled length of the valley. Radial velocities measured within the valley by the DOW were directed towards the radar looking up the valley (Fig. 2(b)) and away from the radar at azimuths pointing down the valley (Fig. 2(c)). The radar reflectivity displayed in the vertical cross-sections up and down the valley shows a clear bright band marking the melting layer at approximately 2 km altitude at this time (Figs. 2(b) and (c)). The radial velocity field shows that the flow was down the valley below, and up-valley above, the melting level. The abrupt changeover from down- to up-valley flow near the melting level was typical of DOW observations in MAP, and suggests that melting of precipitation particles may

* All heights are above mean sea level except where indicated.

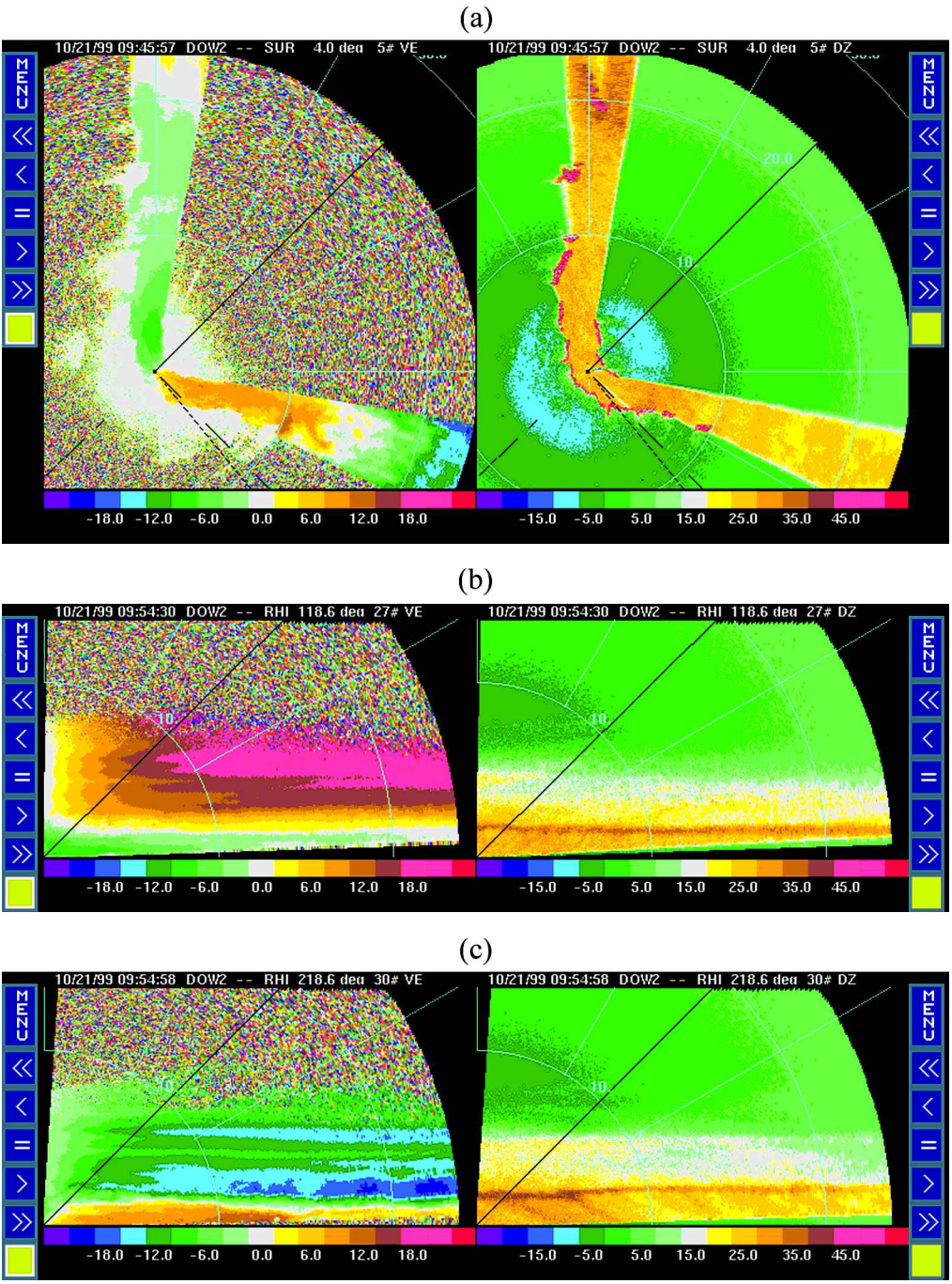

Figure 2. Radar images collected on 21 October 1999 in the Toce river valley: (a) 0945 UTC low-elevation (4 degrees) surveillance scan (PPI); (b) 0954 UTC vertical cross-section (RHI) in the direction up the Toce river valley towards Domodossola; (c) as (b) but in the direction down the Toce river valley towards the Lago Maggiore. The ground-based DOW radar was located at the Pieve Vergonte site (centre of the polar grid in (a), and lower-left corner in (b) and (c)). In each case radial Doppler velocity (m s^{-1}) is shown in the left panel and radar reflectivity (dBZ) in the right panel. Range rings are indicated every 10 km.

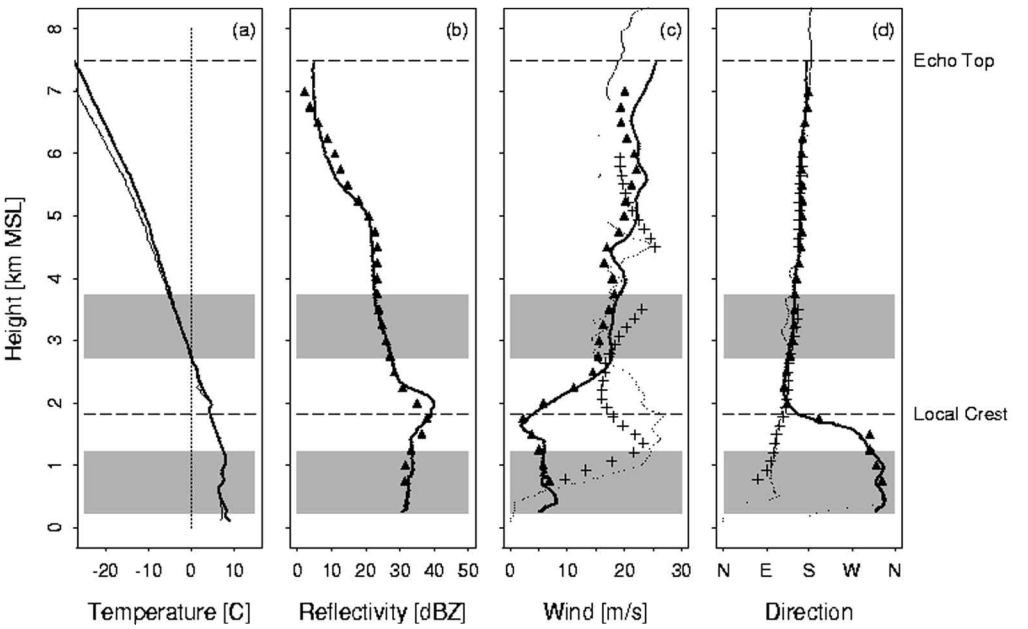

Figure 3. Vertical profiles of temperature, precipitation, and wind structure as recorded by: the atmospheric sounding launched at 1200 UTC from Milano-Linate airport (dotted lines); the UHF wind profiler at Lonate Pozzolo (crosses); the ground-based DOW Doppler radar deployed within the Toce river valley (solid lines); and the airborne Doppler radar above the Toce river valley (solid triangles). All measurements were at about 0950 UTC 21 October 1999. Shown are (a) temperature and dew-point temperature from the sounding; (b) radar reflectivities from the DOW and airborne radars; (c) wind speed, and (d) wind direction, both from DOW and airborne radars, UHF profiler and sounding. The shaded altitude ranges indicate the profile averages used in Fig. 6 for the 'within valley' and 'above local crest line' conditions, avoiding the winds in the transition zone.

be physically related to the airflow in the valley. The fallstreaks seen in the reflectivity field below the bright band are consistent with the vertical shear displayed in the flow field.

Figure 3 shows the thermodynamic stratification upstream of the Alps (as represented by the noon sounding from Milano and the UHF wind profiler at Lonate Pozzolo) and in the Toce valley (via winds profiled by the DOW and P-3 Doppler radars) at about 0950 UTC 21 October 1999. The Milano sounding shows saturated conditions through the lowest few kilometres (Fig. 3(a)), and a particularly stable stratification evidenced in the lowest kilometre. The vertical profile of reflectivity observed by the ground-based (DOW, solid line) and airborne (P-3, solid triangles) radars (Fig. 3(b)) in the Toce river valley is typical of stratiform precipitation, with a bright band forming a few hundred metres below the 0 °C level in the Milano sounding (Fig. 3(a)). The radar echoes topped at about 7–8 km (based on where the reflectivity starts deviating from the clear-air background signal). In stratiform precipitation, particles grow primarily by deposition of water vapour and aggregation while settling downwards (Houze 1981, 1993).

The vertical profile of horizontal winds above the DOW site (derived by VAD analysis) is shown in Figs. 3(c) and (d). The wind speed and direction revealed by the airborne radar (solid triangles) closely mirror those observed from the ground (solid line). The wind speed at this location within the valley was approximately 5 m s^{-1} from a northerly direction (i.e. down the valley), with a weakly defined speed maximum within the lowest 300 m above the surface. The local crest line (i.e. marking the uppermost extent of the Toce valley's walls) is at approximately 1800 m. The wind

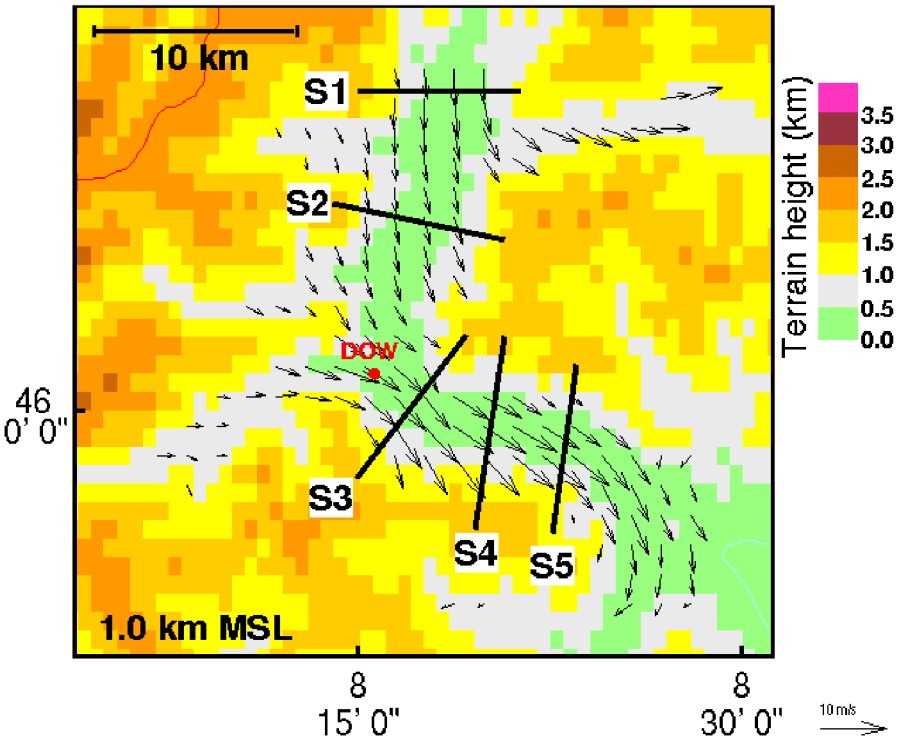

Figure 4. Wind field within the Toce river valley and its tributaries as depicted by the airborne dual-Doppler analysis based on the 0949–0954 UTC P-3 flight leg on 21 October 1999. The horizontal grid resolution is 500 m, and only one out of every four wind vectors is plotted. S1 to S5 indicate the locations of vertical cross-sections referred to in Fig. 5.

speed above that level was significantly larger (15–25 m s^{-1}) and from a south-easterly direction. Above 3 km, the winds measured by the DOW and P-3 Doppler radars are in close agreement with those observed by the upstream sounding and profiler (dotted line and crosses in Figs. 3(c) and (d)), consistent with a greatly reduced influence of the terrain. Below 3 km, however, the sounding and profiler data within the Po basin showed strong (25 m s^{-1}) east-south-easterly winds suggestive of blocked flow upstream of the mountains (Rotunno and Ferretti 2001). Within the lowest several hundred metres those winds were quite weak, consistent with the observed, highly stable atmospheric stratification (Fig. 3(a)). As shown by the more comprehensive dual-Doppler measurements (Bousquet and Smull 2003), this flow was profoundly blocked and thus unable to rise directly over the steep terrain. Rather, it was the ascent of air found above 1 km in the Milano sounding that evidently resulted in the persistent and widespread moderate rainfall both over and well upstream of the Alpine barrier.

A 3D perspective of the down-valley airflow is provided by the airborne dual-Doppler radar data. During IOP 8 the NOAA P-3 aircraft made two passes (between 0911–0916 and 0949–0954 UTC) that afforded views into the Toce river valley. Figure 4 illustrates the fidelity of the airborne Doppler-derived winds within the Toce river valley and its tributaries for the latter overpass. In addition, Fig. 4 reveals important details not evident from a fixed, ground-based single-Doppler perspective. Several tributaries (most notably the Valle Anzasca, which joins the Toce valley near the DOW location at Pieve Vergonte) clearly constituted localized sources of westerly down-valley flow

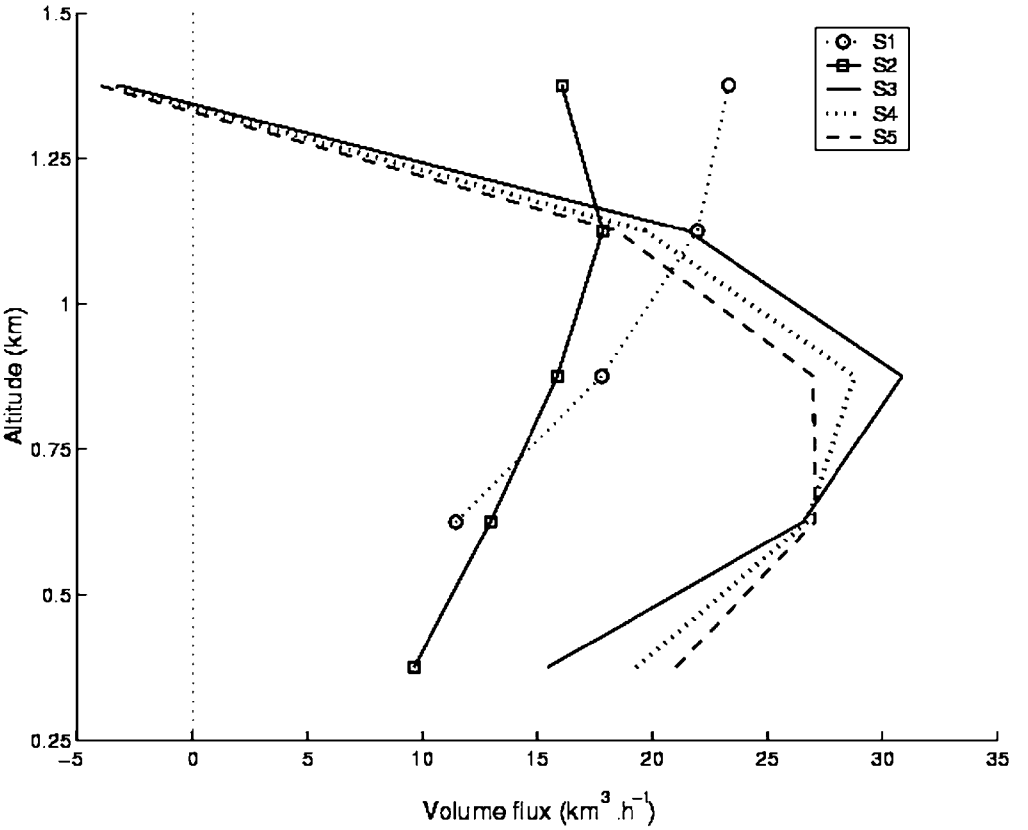

Figure 5. Profiles of horizontal air volume flux at the Toce river valley cross-sections S1 to S5 shown in Fig. 4. These profiles are based on the airborne dual-Doppler analysis of the 0949–0954 UTC P-3 flight leg on 21 October 1999. Plotted values represent contributions over layers 250 m deep in the vertical. Positive values denote down-valley flow.

that merged with more northerly winds along the main stem of the Toce river valley. In contrast, the saddle (altitude 830 m) from the Valle Vigezzo (which extends eastward from the Toce north of Domodossola) into the Centovalli evidently provided an alternate escape route for a portion of the down-valley flow generated within the Toce drainage. An abrupt flow transition detected near the mouth of the Toce shows the merger of down-valley winds with the easterly-component flow that blanketed the Po basin at low levels. The profoundly blocked nature of this larger-scale upstream flow is explored further by Bousquet and Smull (2003).

The important role of tributaries (i.e. side valleys) in inducing variations of down-valley flow strength along the Toce's ~50 km sampled length is illustrated in Fig. 5, which presents mean volume flux profiles through five valley cross-sections (S1–S5 in Fig. 4) derived from the airborne dual-Doppler analysis. At the lowest sampled levels (i.e. below 500 m from S2 to S5) airborne observations show a monotonic increase in the down-valley flux with distance from the Alpine crest toward the valley mouth. Given the valley's relatively constant cross-sectional area (approximately 4 km^2 as measured below 1.25 km), this increase was largely associated with growing strength of the mean down-valley flow component as air fed towards the Po basin. For example, between the surface and 1.25 km the mean down-valley flow component increased from

$\sim$3.5 m s^{-1} at S2 to $\sim$7.5 m s^{-1} at S5. This increase did not proceed in linear fashion, but rather appeared to respond to the influence of the Toce's tributaries. In particular, a significant increase in down-valley flux between S2 and S3 coincided with an input flux of 30 km^{3}h^{-1} from two intervening tributaries feeding toward the DOW's location from the west (the Valle Anzasca and nearby Valle d'Antrona). Likewise, a further complicating factor in the upper reaches of the Toce valley was the escape of air (above 800 m) eastward through the Valle Vigezzo into the Centovalli (Fig. 4), which evidently accounted for the observed slight reduction in down-valley flux between S1 and S2. The total flux of down-valley flow emerging from the mouth of the Toce at this time was approximately 95 km^{3}h^{-1}, in good agreement with independent estimates from the DOW discussed later. Above 600 m, a reversal of this monotonic trend (toward decreasing down-valley flow strength in proximity to the valley's mouth) and extreme vertical shear reflects the influence of the overlying upslope-directed flow approaching from the Po basin. The marked difference above 1 km between the vertical volume flux profiles observed in the upper part of the Toce valley (S1 and S2) and those in the lower part (S3, S4, and S5) highlights the varied degree of exposure to the upslope flow.

Figure 6 shows a time-series analysis of the surface winds and precipitation within the Toce valley from 12 UTC 20 October 1999 until 12 UTC 22 October 1999, in conjunction with DOW-derived winds (averaged over both a near-surface layer and an elevated layer above the confines of the valley) for an intermediate $\sim$24 h period beginning at 2000 UTC 20 October. In addition, the UHF profiler winds at the elevated layer (3.3 km) are shown. The DOW observations reveal a significant down-valley flow of approximately 5 m s^{-1} within the lowest 1 km, consistent with the down-valley flow indicated by the surface weather station near the DOW's location (Figs. 6(a) and (b)). The DOW observations began at the time the air motion within the valley switched from up- to down-valley flow (Fig. 6(b)). The down-valley flow was initially confined to the lowest kilometre but eventually deepened to fill the entire valley. This trend is also evident from comparison of airborne Doppler measurements within the Toce at 0914 (not shown) and 0952 UTC (Figs. 4 and 5). The vertical extent of the down-valley flow in IOP 8, however, never reached above the height of the radar bright band within the Toce valley. Maximum wind speeds of approximately 10 m s^{-1} were found a few hundred metres above the valley floor (Fig. 3(c)). Above the local crest line, a southerly upslope jet (gradually backing to south-easterly with time) pushed moist air towards the Alpine barrier with maximum wind speeds of 25 m s^{-1}, producing this very persistent rainfall in the region (Figs. 3, 6(a) and (b)).

The bright band, initially at about 1 km above the ground, rose to above 2 km (i.e. slightly exceeding the local crest line of the Toce valley) within 24 h (Fig. 6(c)). Assuming adiabatic conditions (i.e. 0.6 K per 100 m altitude difference), the rise in bright-band height of 1.3 km corresponded to a local temperature increase of 7.8 K, which was also reflected in the surface temperature observations. Thus, in concert with the shift of the upslope wind from a southerly to south-easterly direction (after 0600 UTC 21 October), increasingly warmer and correspondingly moister air was pushed against the Alps. Precipitation during this event was light to moderate, with maximum rain rates of 5 mm h^{-1}, but very widespread and persistent, accumulating close to 80 mm of rain in two days (Fig. 6(d)). The higher rain rates on the ground were observed during times of deeper clouds (i.e. maximum echo-top height).

The air motion within the valley reversed from up- to down-valley flow after a few hours of rain (notably *before* the upslope wind direction changed markedly) and eventually began to switch back after the rainfall ceased (Figs. 6(b) and (d)). The surface temperature in the Toce valley decreased approximately 1 K during the first 6 h of

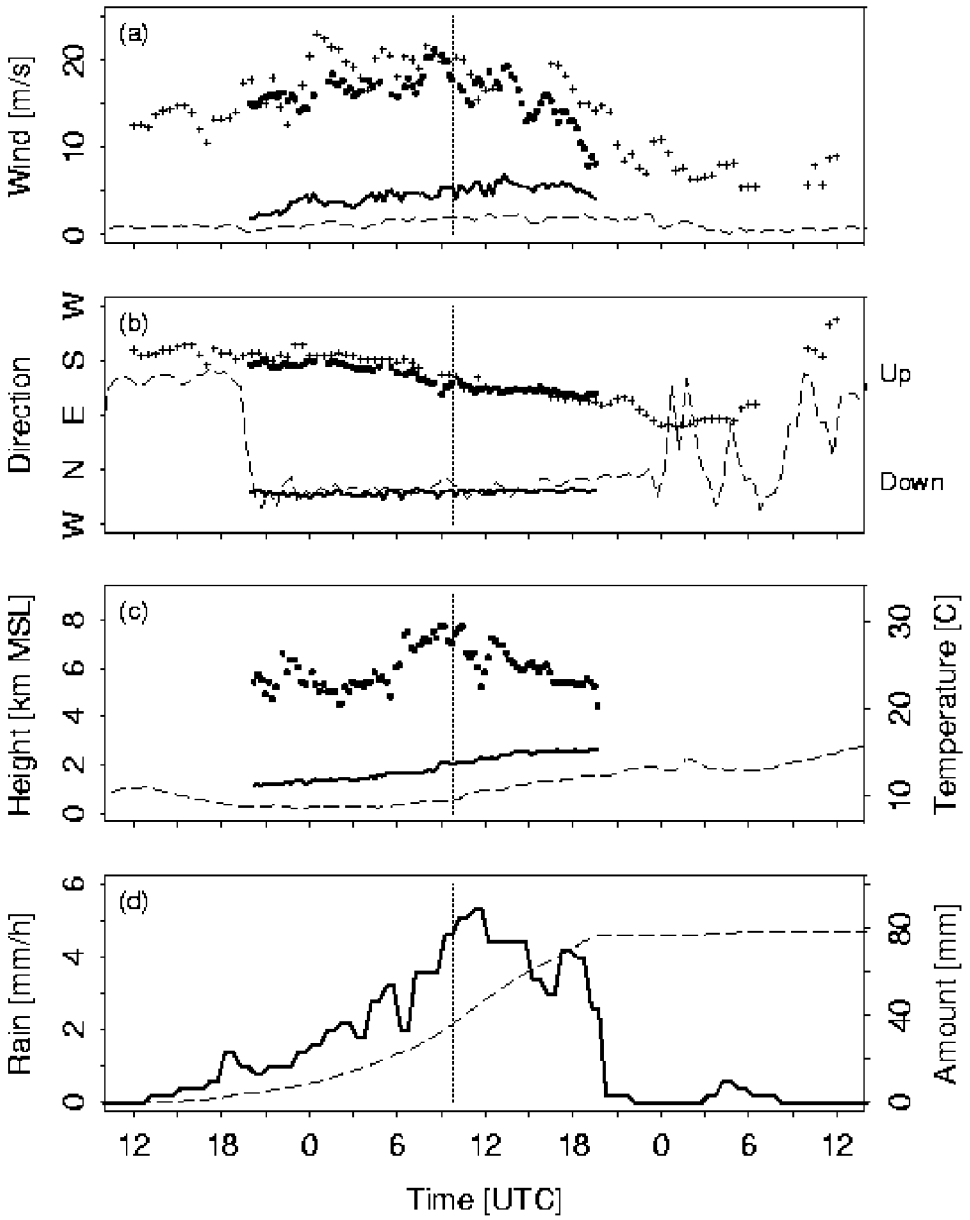

Figure 6. Time series for the heavy rainfall event of 20–22 October 1999. (a) Wind speed, and (b) wind direction: surface wind observations (dashed lines); above the crest line (dots) and within the Toce river valley (bold line) as seen by the mobile ground-based Doppler radar (DOW; see Fig. 3 for corresponding altitude ranges); UHF wind profiler observations at approximately 3.3 km (crosses). (c) Temperature (dashed line) and precipitation echo structure: echo top (dots) and bright-band height (bold line) are based on radar observations. (d) Surface rainfall traces: rainfall rate (bold line, left-hand scale); cumulative amount (dashed line, right-hand scale). The vertical dotted line at 0950 UTC 21 October 1999 indicates the time of the vertical profiles of the DOW radar data shown in Fig. 3.

rainfall and subsequently remained roughly constant until 0600 UTC 21 October, when the upslope wind direction started to change notably. The few hours of light rainfall in the early morning of 22 October appear to have caused some additional flow down the valley (also marked by a slight surface temperature depression). This raises an important question about the physical mechanism behind this down-valley flow: could cooling of the air by melting and evaporation, plus the drag of falling raindrops, have resulted in enough subsidence of air to cause this persistent down-valley flow?

In a steady, large-scale environment, flow reversal and downslope/down-valley flow (directed opposite to the flow of moist air that is lifted onto the topographic barrier) may be a consequence of either dynamic blocking or locally generated negative buoyancy (e.g. Carbone *et al.* 1995). The latter can be caused by cooling from diabatic processes such as radiation, melting, and/or evaporation. The resulting down-valley flow may exhibit properties consistent with a density or gravity current (e.g. Simpson 1997), where depth and speed of the reversed flow are related to buoyancy. Dynamic blocking is related to the kinetic energy in the upstream flow and the potential energy created by means of lifting under stable stratification. This is commonly treated as a dimensionless Froude number, $Fr = U/NH$, where U is the upstream wind speed component orthogonal to the mountain barrier at a distance $>10H$ with H a characteristic height of the barrier, and N is the Brunt–Vaisala frequency of the lifted layer. A typical feature of low-Fr flow past an ideal 2D topographic barrier is flow stagnation and potential flow reversal on the windward side of the obstacle (e.g. Smith 1980; Smolarkiewicz and Rotunno 1990; Bauer *et al.* 2000). Under such conditions, downslope flow may be observed at low levels, where the flow is essentially blocked from crossing over the barrier.

The rugged terrain of the Alps, which consists of a curved barrier comprising many small-scale ridges and valleys, is far from the above idealized setting. Nonetheless, the atmospheric stability of the upstream airflow could be estimated from the Milano soundings using information in the 925–700 hPa layer and a scaling height of 2500 m (representative of an average height of the Alps in the Lago Maggiore region). For IOP 8, the estimated Froude number ($Fr < 0.5$) indicates a strong potential for upstream flow stagnation and flow reversal. Thus a dynamic blocking effect cannot be ruled out as contributor to the down-valley flow. However, the data shown in Fig. 6 strongly suggest that diabatic processes played a key role. In particular, the flow reversal occurred at a time of strengthening of the upslope flow (see the UHF-based wind speed increase in Fig. 6(a)), which would have presumably increased Fr and thereby *reduced* the potential for dynamic blocking. Moreover, the observed decrease in surface temperature during the first several hours of rainfall indicates that significant cooling occurred (Figs. 6(c) and (d)), as would be expected if diabatic influences were predominant.

The Toce river valley is trapezoid-shaped with a width of approximately 1–2 km at the valley floor and 6–7 km at the local crest line. The vertical cross-section normal to the axis of the valley is approximately 6 km^2. The ratio of the valley width at its crest to the valley depth is about 3–4, indicating a low susceptibility to ambient influences and thus deeper drainage flows (Barr and Orgill 1989). The persistent down-valley flow of 5 m s^{-1}, eventually filling the valley up to the crest, resulted in approximately 100 $km^3 h^{-1}$ of air flowing out from the Toce river valley towards the Lago Maggiore, and this for more than 24 h (Fig. 6(b)). (The relative importance of this local down-valley flow to other regional air motions, and ultimately to the precipitation formation processes, remains to be determined.) At the height of the local crest line, a minimum estimate of the horizontal cross-sectional area of the valley is approximately 350 km^2 (7 km wide and 50 km long), not including any tributaries which might double this

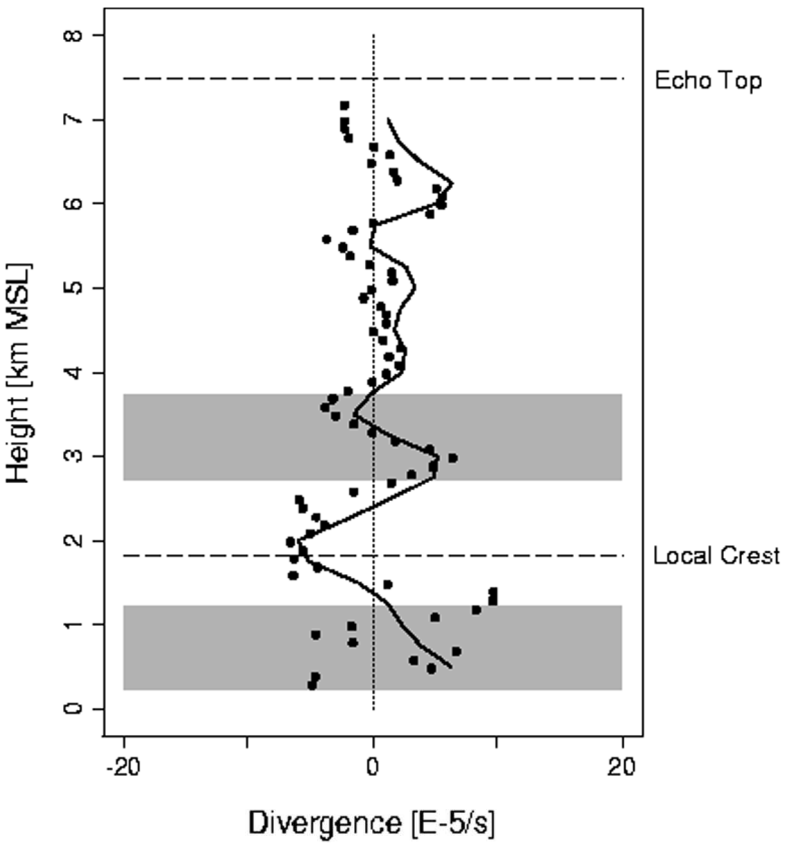

Figure 7. Profile of horizontal divergence (10^{-5} s^{-1}) within and above the Toce river valley based on airborne and ground-based Doppler radar (DOW) analyses at about 0950 UTC 21 October 1999. The DOW analysis (shown by the dots) is based on using the extended VAD technique developed by Matejka and Srivastava (1991). The airborne P-3 dual-Doppler analysis (solid line) is detailed in Smull *et al.* (2000). The shaded altitude ranges are as in Fig. 3.

estimate. Dividing the 100 km^3h^{-1} by 350 km^2 indicates that the rate of subsidence of air over this trapezoid-shaped valley would have to be about 0.3 km h^{-1} ($\sim$0.1 m s^{-1}) to explain the observed flow down and out of the valley. This rate of subsidence is consistent with subsidence produced by the cooling of air from melting and evaporation of precipitation particles (Atlas *et al.* 1969; Zipser 1969, 1977; Leary and Houze 1979; Srivastava 1987; Li and Srivastava 2001). The drag of falling raindrops would reinforce the subsidence produced by cooling.

Leary and Houze (1979) studied the melting and evaporation in stratiform anvil precipitation of MCSs. They estimated a cooling rate from melting of ice particles of approximately 4.5 K h^{-1} (for a 5 mm h^{-1} rain rate), similar in magnitude to the cooling rate derived from evaporation of raindrops below cloud base. For IOP 8, we estimate an average cooling rate from melting of approximately 1.8 K h^{-1} based on a mean rain rate of 2 mm h^{-1} for this event. (The maximum cooling rates from melting were of order 5 K h^{-1}.) Evaporation was likely to be contributing to the cooling effect because the cloud base was below the local crest line but clearly above the valley floor (based on visual observation); however, this cooling could not be quantified owing to a lack of thermodynamic profiling within the valley. The average cooling rate from melting was

of the same order of magnitude as the clear-sky nocturnal long-wave radiation cooling rates of 1–2 K h^{-1} estimated by Orgill *et al.* (1992).

There are similarities between the stratiform precipitation structure found by Leary and Houze (1979) for the stratiform anvil region of tropical MCSs and the upslope orographic precipitation observed during IOP 8 (although we recognize that there are fundamental differences in the circulations and forces). The anvil precipitation exhibits a bright band, like that seen in the right-hand panels of Figs. 2(b) and (c), with rapid changeover from rear-to-front flow (relative to the storm system) below the 0 K level to front-to-rear flow above. The stratiform region of the MCS is characterized by mesoscale ascent above the melting layer, where ice particles grow by vapour deposition (and maybe minimally also by riming) and aggregation, and mesoscale descent below. The downdraughts below the melting layer of MCS anvils typically have magnitudes on the order of tens-of-cm s^{-1} (Gamache and Houze 1982, 1985; Houze and Rappaport 1984; Houze 1989; Mapes and Houze 1995). The corresponding profile of horizontal divergence exhibits a zone of convergence at the melting layer accompanied by divergence above and below (e.g. Houze 1989; Mapes and Houze 1995). The widespread orographic rainfall of 20–22 October 1999 resulted from condensation of moisture in the ascending air above the local crest line forced by the slope of the mountains. Within the valley, cooling from melting and evaporation of precipitation particles falling into the valley evidently led to subsidence. Ground-based single-Doppler and airborne dual-Doppler radar analyses independently reveal the typical layer of convergence at the height of the radar bright band (Fig. 7), accompanied by downward motion of a few tens-of-cm s^{-1} within the valley and upward motion of potentially several tens-of-cm s^{-1} above the crest line (not shown). The latter is in good agreement with updraughts of numerical simulations of the IOP 8 precipitation (see Fig. 9 in Rotunno and Ferretti 2003).

4. Observations in other MAP IOPs

The down-valley flow under heavy rainfall was neither unique to IOP 8 nor to the Toce river valley, but was also observed by the DOW during its deployments in the Ticino river valley (Steiner *et al.* 2000). Inspection of the surface data collected by the Pieve Vergonte hydrometeorological station (near the DOW deployment site) from 29 June to 10 November 1999 inclusive, shows that flow down the valley during rain was not peculiar to IOP 8 but observed as a rather common feature (Fig. 8). Separating the 30-minute samples into rain and no-rain categories shows that the dry airflow within the Toce river valley (at least for the summer and autumn of 1999) is mostly thermally driven—i.e. flow up the valley during the day and down the valley during night-time (Fig. 8(a)). During that 135-day period of observation it was raining only 12% of the time; the total rainfall accumulation was 667 mm. However, when it was raining the flow was predominantly down rather than up the valley (Fig. 8(b)). Removal of the first few hours of rainfall for each event from Fig. 8(b) (plus IOP 2b for reasons discussed later) brings out the down-valley component even more prominently, leaving almost no points in the up-valley direction. There was no diurnal signature apparent in the valley flow under rainfall.

Table 1 summarizes the flow within the Toce river valley, based on the surface observations, for the major rainfall events observed during the SOP. The observed surface winds were significantly weaker than those measured above the valley floor by the DOW (Fig. 6(a)). For all the 11 IOPs listed, down-valley flow was observed under rainfall. For eight of these events (IOPs 2a, 2b, 4, 8, 9, 13, 14, and 15), the flow

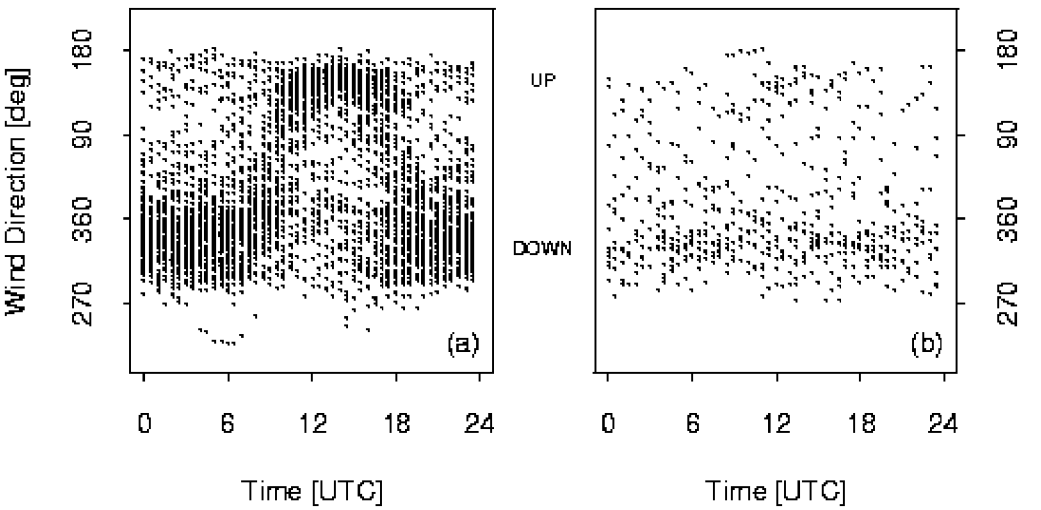

Figure 8. Wind direction analyses for the Toce river valley as a function of time of day for the period 29 June to 10 November 1999 inclusive, separated into: (a) non-raining, and (b) raining conditions.

was initially up the valley, but eventually reversed while it was raining. The up-valley flow direction for those IOPs (except IOPs 2b, 9, and 15) before the rain started was consistent with a thermally driven diurnal cycle for that time of day. The observed night-time down-valley flow for IOP 10 before rain started was also consistent with a thermally driven diurnal cycle. However, this timing may have been coincidental. Synoptic-scale influences on the valley flow have to be considered for situations leading up to heavy rainfall. The cases were associated with significant baroclinic waves, which produced low-level flow from the Mediterranean Sea. Reversal from up- to down-valley directed flow generally occurred only after a few hours of persistent rainfall. Some time was needed to accumulate enough subsided heavier air, cooled by melting and evaporation, to eventually overcome the pressure gradient set up within the valley by the diurnal thermally driven cycle under weak synoptic forcing. For example, note the decreasing surface temperature during the first several hours after the onset of rainfall in IOP 8 (Figs. 6(c) and (d)). Similar temperature decreases during rainfall were observed in other IOPs.

IOP 2b was the greatest rain event of the SOP. This storm had synoptic characteristics and rainfall amounts similar to the Piedmont flood case of 1994 (Buzzi *et al.* 1998; Doswell *et al.* 1998; Rotunno and Ferretti 2001). During the initial 30 h of IOP 2b, the low-level flow was dynamically driven up the valley in connection with the baroclinic wave passing over the region. Both the wind and thermodynamic stratification during this time favoured unblocked ascent of the low-level air mass (Houze *et al.* 2000; Medina and Houze 2003; Rotunno and Ferretti 2003). The flow within the valley was well connected to the flow above the surrounding mountains, going up the valley and presumably surmounting the barrier. During the later hours of the storm, the large-scale flow at low levels may have weakened, eventually setting the stage for the flow to reverse into a down-valley flow. This flow reversal in the Toce valley was again accompanied by a marked drop in surface temperature.

DOW radar observations in the Toce river valley are available for IOPs 8, 9, 10, 14, and 15. The radar bright band (melting layer) during IOPs 8, 9, 10, and 14 was typically

TABLE 1. CHARACTERISTICS OF THE SURFACE AIRFLOW IN THE TOCE RIVER VALLEY UNDER RAINFALL

IOP[1]	Rain (mm)	Cooling (K h^{-1})	Flow direction, strength, and air temperature
2a	4.8	0.9	Flow up the valley when rain started, changing to down-valley flow after a few hours; flow reversal accompanied by a temperature drop; winds generally $\leq$2 m s^{-1}.
2b	250.1	4.5	Flow up the valley >2 m s^{-1} for initial 30 h of heavy rainfall, later changing to down-valley flow $\leq$2 m s^{-1} when Froude number decreased; flow reversal accompanied by a temperature drop.
3	24.0	1.4	Flow down the valley <2 m s^{-1} during rainfall.
4	12.9	1.8	Flow up the valley $\sim$1 m s^{-1} when rain started, changing to down-valley flow $\sim$2 m s^{-1} after a few hours; flow reversal followed by decreasing temperature.
5	7.4	0.5	Flow down the valley $\sim$1 m s^{-1} during rainfall; increasing strength towards end >2 m s^{-1}.
8	78.8	1.8	Flow up the valley $\sim$1 m s^{-1} when rain started, changing to down-valley flow $\leq$2 m s^{-1} after a few hours; temperature decrease leading up to flow reversal.
9	22.5	1.4	Flow up the valley $\sim$1 m s^{-1} when rain started, changing to down-valley flow $\sim$1 m s^{-1} after a few hours; flow reversal followed by decreasing temperature.
10	28.6	0.9	Flow down the valley when rain started (low Froude number) and remaining down-valley $\sim$1 m s^{-1} until towards end of rainfall when Froude number increased and flow reversed to up the valley $\leq$2 m s^{-1}; flow reversal accompanied by a jump in temperature.
13	4.1	0.5	Flow up the valley $\sim$1 m s^{-1} during breaks in rainfall, but down-valley flow when raining $\sim$1 m s^{-1}; temperature decreasing during periods of significant rainfall.
14	44.6	1.4	Flow up the valley $\sim$1 m s^{-1} during breaks in rainfall, but down-valley flow when raining $\leq$2 m s^{-1}; temperature decreasing during periods of significant rainfall.
15	18.0	2.7	Flow up the valley $\sim$3 m s^{-1} when rain started, changing to down-valley flow <4 m s^{-1} after cold front crossed Alps and pushed downslope and throughout the valley; flow reversal accompanied by a temperature drop.

[1] Intensive Observing Period.

at an altitude of approximately 2 km (except in IOP 8, where it was initially at a lower level), which is directly above the local crest line of the Toce river valley in the vicinity of the DOW's deployment location. The maximum depth of the down-valley flow never reached the height of the radar bright band, and only in IOP 8 did it eventually fill the entire depth of the Toce valley. Moreover, the strength and depth of the flow down the valley were related: the strongest and deepest down-valley flow was observed in IOP 8, followed by IOPs 14, 9, and 10. This order agrees well with the rainfall amounts (as a proxy for the negative buoyancy caused by the cooling from melting and evaporation) observed during these events (Table 1).

During IOP 15, a very intense cold front crossed the Alpine barrier from the north and forced itself under an equally strong southerly upslope flow, thus reversing a flow initially up the Toce river valley into a down-valley flow. Although clouds and precipitation-sized particles were generated within the upslope flow, the rain falling into the Toce river valley evaporated almost entirely within the cold and dry air following the passage of the front. The radar bright band was initially at approximately crest height, but lowered to an altitude of 1 km during the event. IOP 15 was the only case

where DOW observations revealed a flow in the down-valley direction that was neither confined to heights below the radar bright band nor the depth of the Toce river valley. In fact, the downslope/down-valley flow reached depths of 4–5 km (i.e. the maximum height of the Alpine barrier). Such a phenomenon is typically referred to as severe downslope wind or bora (e.g. Smith 1985, 1987; Colle and Mass 1998; Lazic and Tošic 1998).

The large-scale dynamic blocking effect was estimated, based on the dry Froude number characterizing the upstream airflow and derived from the Milano soundings. Typically the Froude number was ≤ 0.5 during rainfall (except IOPs 2b and 10), indicating a potential for upstream flow stagnation and flow reversal. Whenever $Fr > 0.5$, the flow within the valley behaved more similarly to the upslope flow aloft (i.e. it was directed up-valley). However, there are several significant caveats to consider: (i) the Froude number computations based on the Milano soundings are very sensitive to the altitude range selected, the scaling height used, and whether or not moisture was considered for estimating the Brunt–Vaisala frequency (e.g. Durran and Klemp 1982); (ii) the Milano soundings may not have sampled the upstream conditions well for all the IOPs listed in Table 1, and the number of soundings collected for any given storm may be too small to be meaningful; and (iii) the Froude number is a highly idealized quantity most easily interpreted in terms of flow over a smooth 2D barrier. Relating Froude numbers estimated from a few isolated soundings to flow over a rugged and curved 'real world' barrier is highly questionable.

Estimates of locally generated negative buoyancy were based on the cooling from melting of snow using an average rainfall rate (Table 1). The true cooling was probably larger because of contributions from evaporation, which could not be estimated. Significant cooling from melting (and evaporation) occurred in most of the events and was typically on the order of 1–2 K h^{-1}. Evidence of this cooling was revealed, particularly during flow reversals, as air flowing down the valley was demonstrably cooler than the air going up the valley.

The results summarized in Table 1 indicate that dynamic blocking effects may have influenced the direction of the airflow within the Toce river valley. However, diabatic processes almost certainly played a major role in generating negative buoyancy and were likely to have been the key driving mechanism behind many of the observed down-valley flows.

5. Conclusions

Our analyses of the airflow within the Toce river valley, based on ground-based and airborne Doppler radar, surface, and upper-air data collected during MAP show that precipitation can strongly modify the airflow within valleys.

Melting and evaporation of precipitation particles result in cooling of air. The cooling from melting is primarily confined to the height of the melting layer (indicated by the radar bright band), and cooling from evaporation is typically confined to the altitude range below cloud base. Cooling from melting results in the development of a 0 °C isothermal layer destabilizing the layer below and mixing the cooling effects downwards. Cooled air is heavier than its environment and thus starts to subside. Evaporation will contribute to enhance this downward motion. In the absence of forces other than gravity, the subsiding air concentrates in river valleys, which act as air drainage channels. Down-valley flow generated this way is driven by gravitational force and may thus be termed drainage flow (Steiner *et al.* 2002), similar to the nocturnal drainage flow under clear sky and weak synoptic conditions. The difference between

the *wet* and *dry* drainage flows is in the mechanism causing the air to subside: cooling by melting and evaporation during wet conditions, and by long-wave radiation under dry conditions. The cooling rates from melting and evaporation may exceed those resulting from nocturnal, clear-sky radiation cooling. While a dry drainage flow may occur at night-time during periods of weak synoptic forcing, wet drainage flows are not bound to night-time and may overcome moderate synoptic forcing.

Observations made during the SOP show that a down-valley drainage flow can develop underneath an opposite-directed flow of moist air that is lifted onto the topographic barrier. This will occur in situations where the lowest boundary-layer air remains blocked and only air from layers above 1–2 km may rise over the barrier. In the absence of atmospheric instability, this results in widespread upslope (orographic) precipitation, where particles are formed in the air ascending the slope of the terrain. The melting layer (indicated by the radar bright band and dynamically marked by a layer of convergence) tends to separate the upward motion above from the downward motion below it. The process generating subsidence of air by cooling from melting and evaporation of precipitation particles resembles the production of a mesoscale downdraught in the stratiform anvil region of a MCS. (Similar processes are also at play generating severe downdraughts in thunderstorms.) Sustained orographic precipitation will be accompanied by subsiding air that becomes concentrated in valleys and results in a drainage flow. This precipitation-driven drainage flow may reach a maximum depth limited primarily by the height of the melting layer and secondarily by the valley confines. The drainage flow strength and depth are related to the rainfall amount, and within the valley appears to be disconnected from the larger-scale upslope flow. Examples of wet drainage flow documented in MAP include IOPs 8, 9, 10, and 14.

The flow within a valley may initially be up the valley when rain starts. The time delay of flow reversal after the onset of rain depends on the precipitation intensity, the degree of subsaturation below cloud base, and the strength of the ambient up-valley pressure gradient. The effect of the cooling-induced subsidence, however, may not be strong enough to result in the reversal of an up-valley flow into a down-valley flow under strong dynamic forcing conditions, unless the synoptic-scale pressure gradient along the valley axis weakens with time. (The process may happen in reverse order as well.) Moreover, atmospheric instability may provide enough vertical overturning of air to prohibit the development of the disconnection of flow within a valley from the flow above the valley confines; IOP 2b is an example of that.

Alternatively, a down-valley flow may also be generated under strong dynamic forcing, for example when an intense cold front crosses the Alpine barrier forcing itself under a potentially equally strong upslope moist air stream in which precipitation is generated (IOP 15). In this case, the flow down the valley may have significant depth and clearly exceed the melting layer (bright band) and the valley confines. However, this is not a drainage flow; such a phenomenon is typically referred to as severe downslope wind or bora.

And last but not least, the analyses presented demonstrate the utility of mobile ground-based and airborne Doppler radar measurements to specify details of the airflow structure and its evolution within complex terrain.

Future observational programmes should aim to substantiate this view of the flow in valleys under precipitation. Particular attention should be paid to the thermodynamic profiling upstream and within valleys. Moreover, numerical simulations may serve to further quantify the various effects of cooling by melting and evaporation, and putting them in perspective with the diurnal thermal (i.e. heating/cooling) effects and the dynamic forcing imposed upon the valley.

The contribution of precipitation-induced down-valley flows to larger-scale blocking upstream of the Alpine barrier, which could significantly impact the spatial distribution of orographic rainfall, remains to be determined through analysis of more spatially extensive ground-based and airborne dual-Doppler datasets collected during MAP.

Acknowledgements

We are grateful to MyShelle Bryant, Scott Richardson, Seth Noble, and Celia Jones for their expertise and endurance during long-lasting DOW operation periods, and Joshua Wurman for facilitating the DOW for MAP. Messrs Aerni and Blardone are gratefully acknowledged for allowing us to operate the DOW radar on their farms. In addition, we thank the authority of the Lodrino and Magadino airports, and Mr Caputo of the Centrale Edison, for providing us access to restricted areas facilitating our operations. The exceptional local knowledge and logistical assistance provided by Jürg Joss was key to the success of the DOW operations during MAP and is deeply appreciated. The thoughtful comments by Richard Carbone and an anonymous reviewer were very welcome. Richard Rotunno contributed stimulating discussions. Socorro Medina carried out the sounding analyses. The sounding and profiler data were obtained from the MAP Data Center. The manuscript was carefully proof-read by Mary Steiner. This research was supported by the National Science Foundation under grants ATM-9906012 (Smith and Steiner) to Princeton University, and ATM-9817700 (Houze) and ATM-987502 (Smull) to the University of Washington.

References

Astling, E. G. 1984 On the relationship between diurnal mesoscale circulations and precipitation in a mountain valley. *J. Clim. Appl. Meteorol.*, **23,** 1635–1644

Atlas, D., Tatehira, R., Srivastava, R. C., Marker, W. and Carbone, R. E. 1969 Precipitation-induced mesoscale wind perturbations in the melting layer. *Q. J. R. Meteorol. Soc.*, **95,** 544–560

Banta, R. and Cotton, W. R. 1981 An analysis of the structure of local wind systems in a broad mountain basin. *J. Appl. Meteorol.*, **20,** 1255–1266

Barr, S. and Orgill, M. M. 1989 Influence of external meteorology on nocturnal valley drainage winds. *J. Appl. Meteorol.*, **28,** 497–517

Bauer, M. H., Mayr, G. J., Vergeiner, I. and Pichler, H. 2000 Strongly nonlinear flow over and around a three-dimensional mountain as a function of the horizontal aspect ratio. *J. Atmos. Sci.*, **57,** 3971–3991

Bougeault, P., Binder, P., Buzzi, A., Dirks, R., Houze, R., Kuettner, J., Smith, R. B., Steinacker, R. and Volkert, H. 2001 The MAP Special Observing Period. *Bull. Am. Meteorol. Soc.*, **82,** 433–462

Bousquet, O. and Chong, M. 1998 A multiple-Doppler synthesis and continuity adjustment technique (MUSCAT) to recover wind components from Doppler radar measurements. *J. Atmos. Oceanic Technol.*, **15,** 343–359

Bousquet, O. and Smull, B. F. 2003 Observations and impacts of upstream blocking during a widespread orographic precipitation event. *Q. J. R. Meteorol. Soc.*, **129,** 391–409

Browning, K. A. and Wexler, R. 1968 The determination of kinematic properties of a wind field using Doppler radar. *J. Appl. Meteorol.*, **7,** 105–113

Buzzi, A. and Foschini, L. 2000 Mesoscale meteorological features associated with heavy precipitation in the southern Alpine region. *Meteorol. Atmos. Phys.*, **72,** 131–146

Buzzi, A., Tartaglione, N. and Malguzzi, P. 1998 Numerical simulations of the 1994 Piedmont flood: Role of orography and moist processes. *Mon. Weather Rev.*, **126,** 2369–2383

Caccia, J.-L., Aubagnac, J.-P., Béthenod, G., Bourdier, C., Bruzzese, E., Campistron, B., Candusso, J.-P., Cherel, G., Claeyman, J.-P., Conrad, J.-L., Cordesses, R., Currier, P., Derrien, S., Despaux, G., Dole, J., Durbe, R., Fournet-Fayard, J., Frappier, A., Ghio, F., Girard-Ardhuin, F., Jacoby-Koaly, S., Klaus, V., Ney, R., Pagès, J.-P., Petitdidier, M., Pointin, Y., Richard, E., Seloyan, I., Smaïni, L. and Wilson, R. 2001 The French ST-radar network during MAP: Observational and scientific aspects. *Meteorologische Zeitschrift*, **10,** 469–478

Carbone, R. E., Cooper, W. A. and Lee, W.-C. 1995 Forcing of flow reversal along the windward slopes of Hawaii. *Mon. Weather Rev.*, **123,** 3466–3480

Carbone, R. E., Tuttle, J. D., Cooper, W. A., Grubišić, V. and Lee, W. C. 1998 Trade wind rainfall near the windward coast of Hawaii. *Mon. Weather Rev.*, **126,** 2847–2863

Caton, P. G. F. 1963 'The measurement of wind and convergence by Doppler radar'. Pp. 290–296 in Proceedings of the 10th weather radar conference, Washington DC. American Meteorological Society, Boston, USA

Colle, B. A. and Mass, C. F. 1998 Windstorms along the western side of the Washington Cascade Mountains. Part II: Characteristics of past events and three-dimensional idealized simulations. *Mon. Weather Rev.*, **126,** 53–71

Desiato, F., Finardi, S., Brusasca, G. and Morselli, M. G. 1998 TRANSALP 1989 experimental campaign. Part I: Simulation of 3D flow with diagnostic wind field models. *Atmos. Environ.*, **32,** 1141–1156

Dosio, A., Emeis, S., Graziani, G., Junkermann, W. and Levy, A. 2001 Assessing the meteorological conditions of a deep Italian Alpine valley system by means of a measuring campaign and simulations with two models during a summer smog episode. *Atmos. Environ.*, **35,** 5441–5454

Doswell, C. A., Ramis, C., Romero, R. and Alonso, S. 1998 A diagnostic study of three heavy precipitation episodes in the western Mediterranean region. *Weather and Forecasting*, **13,** 102–124

Durran, D. R. and Klemp, J. B. 1982 On the effects of moisture on the Brunt–Vaisala frequency. *J. Atmos. Sci.*, **39,** 2152–2158

Frei, C. and Schär, C. 1998 A precipitation climatology of the Alps from high-resolution rain-gauge observations. *Int. J. Climatol.*, **18,** 873–900

Frey, K. 1953 Die Entwicklung des Süd- und des Nordföhns. *Archiv für Meteorologie, Geophysik und Bioklimatologie, Serie A: Meteorologie und Geophysik*, **5,** 432–477

Gabella, M. and Mantonvani, R. 2001 The floods of 13–16 October 2000 in Piedmont (Italy): Quantitative precipitation estimates using radar and a network of gauges. *Weather*, **56,** 337–343

Gamache, J. F. and Houze Jr, R. A. 1982 Mesoscale air motions associated with a tropical squall line. *Mon. Weather Rev.*, **110,** 118–135

1985 Further analysis of the composite wind and thermodynamic structure of the 12 September GATE squall line. *Mon. Weather Rev.*, **113,** 1241–1259

Georgis, J. F., Roux, F. and Hildebrand, P. H. 2000 Observation of precipitating systems over complex orography with meteorological Doppler radars: A feasibility study. *Meteorol. Atmos. Phys.*, **72,** 185–202

Grossman, R. L. and Durran, D. R. 1984 Interaction of low-level flow with the western Ghat Mountains and offshore convection in the summer monsoon. *Mon. Weather Rev.*, **112,** 652–672

Hildebrand, P. H., Walther, C. A., Frush, C. L., Testud, J. and Baudin, F. 1994 The Eldora/Astraia airborne Doppler weather radar—goals, design, and first field-tests. *Proc. IEEE*, **82,** 1873–1890

Hill, G. E. 1978 Observations of precipitation-forced circulations in winter orographic storms. *J. Atmos. Sci.*, **35,** 1463–1472

Houze Jr, R. A. 1981 Structures of atmospheric precipitation systems: A global survey. *Radio Sci.*, **16,** 671–689

Houze Jr, R. A. 1989 Observed structure of mesoscale convective systems and implications for large-scale heating. *Q. J. R. Meteorol. Soc.*, **115,** 425–461

1993 *Cloud dynamics*. International Geophysics Series, Vol. 53, Academic Press, San Diego, USA

Houze Jr, R. A. and Rappaport, E. N. 1984 Air motions and precipitation structure of an early summer squall line over the eastern tropical Atlantic. *J. Atmos. Sci.*, **41,** 553–574

Houze Jr, R. A., Medina, S. and Steiner, M. 2000 'Two cases of heavy rain on the Mediterranean side of the Alps in MAP'. Pp. 1–5 in Preprints of the 9th Conference on mountain meteorology, Aspen, Colorado. American Meteorological Society, Boston, USA

Houze Jr, R. A., James, C. N. and Medina, S. 2001 Radar observations of precipitation and airflow on the Mediterranean side of the Alps: Autumn 1998 and 1999. *Q. J. R. Meteorol. Soc.*, **127,** 2537–2558

Jorgensen, D. P., Matejka, T. and DuGranrut, J. D. 1996 Multi-beam techniques for deriving wind fields from airborne Doppler radars. *Meteorol. Atmos. Phys.*, **59,** 83–104

Lammert, L. 1920 Der mittlere Zustand der Atmosphäre bei Südföhn. *Veröffentlichungen des Geophysikalischen Instituts der Universität Leipzig*, Band **2,** Heft 7, 261–322

Lazic, L. and Tošic, I. 1998 A real data simulation of the Adriatic bora and the impact of mountain height on bora trajectories. *Meteorol. Atmos. Phys.*, **66,** 143–155

Leary, C. A. and Houze Jr, R. A. 1979 Melting and evaporation of hydrometeors in precipitation from the anvil clouds of deep tropical convection. *J. Atmos. Sci.*, **36,** 669–679

Lhermitte, R. M. and Atlas, D. 1961 'Precipitation motion by pulsed Doppler radar'. Pp. 218–223 in Proceedings of the 9th weather radar conference, Kansas City, Missouri. American Meteorological Society, Boston, USA

Li, J.-G. and Atkinson, B. W. 1999 Transition regimes in valley airflows. *Boundary-Layer Meteorol.*, **91,** 485–411

Li, X. and Srivastava, R. C. 2001 An analytical solution for raindrop evaporation and its application to radar rainfall measurements. *J. Appl. Meteorol.*, **40,** 1607–1616

McKee, T. B. and O'Neal, R. D. 1989 The role of valley geometry and energy budget in the formation of nocturnal valley winds. *J. Appl. Meteorol.*, **28,** 445–456

Mapes, B. E. and Houze Jr, R. A. 1995 Diabatic divergence profiles in western Pacific mesoscale convective systems. *J. Atmos. Sci.*, **52,** 1807–1828

Marwitz, J. D. 1980 Winter storms over the San Juan Mountains. Part I: Dynamical processes. *J. Appl. Meteorol.*, **19,** 913–926

Matejka, T. J. and Srivastava, R. C. 1991 An improved version of the extended velocity–azimuth display analysis of single-Doppler radar data. *J. Atmos. Oceanic Technol.*, **8,** 453–466

Medina, S. and Houze Jr, R. A. 2003 Air motions and precipitation growth in Alpine storms. *Q. J. R. Meteorol. Soc.*, **129,** 345–371

Neff, W. D. 1990 Remote sensing of atmospheric processes over complex terrain. Pp. 173–228 in *Atmospheric processes over complex terrain*. Ed. W. Blumen. Meteorological Monographs, Vol. 23, No. 45. American Meteorological Society, Boston, USA

Neinman, P. J., Ralph, F. M., White, A. B., Kingsmill, D. E. and Persson, P. O. G. 2002 The statistical relationship between upslope flow and rainfall in California's coastal mountains: Observations during CALJET. *Mon. Weather Rev.*, **130,** 1468–1492

Ohata, T., Higuchi, K. and Ikegami, K. 1981 Mountain-valley wind system in the Khumbu Himal, East Nepal. *J. Meteorol. Soc. Jpn*, **59,** 753–762

Orgill, M. M., Kincheloe, J. D. and Sutherland, R. A. 1992 Mesoscale influences on nocturnal valley drainage winds in western Colorado valleys. *J. Appl. Meteorol.*, **31,** 121–141

Post, M. J. and Neff, W. D. 1986 Doppler lidar measurements of winds in a narrow mountain valley. *Bull. Am. Meteorol. Soc.*, **66,** 274–281

Rotunno, R. and Ferretti, R. 2001 Mechanisms of intense Alpine rainfall. *J. Atmos. Sci.*, **58,** 1732–1749

2003 Orographic effects on rainfall in MAP cases IOP 2b and IOP 8. *Q. J. R. Meteorol. Soc.*, **129,** 373–390

Schneidereit, M. and Schär, C. 2000 Idealised numerical experiments of Alpine flow regimes and southside precipitation events. *Meteorol. Atmos. Phys.*, **72,** 233–250

Seibert, P. 1990 South Foehn studies since the ALPEX experiment. *Meteorol. Atmos. Phys.*, **43,** 91–103

Simpson, J. E. 1997 *Gravity currents in the environment and the laboratory*. Cambridge University Press, Cambridge, UK

Smith, R. B. 1980 Linear theory of stratified hydrostatic flow past an isolated mountain. *Tellus*, **32,** 348–364

1985 On severe downslope winds. *J. Atmos. Sci.*, **42,** 2597–2603

1987 Aerial observations of the Yugoslavian bora. *J. Atmos. Sci.*, **44,** 269–297

Smolarkiewicz, P. K. and Rotunno, R. 1990 Low Froude number flow past three-dimensional obstacles. Part II: Upwind flow reversal zone. *J. Atmos. Sci.*, **47,** 1498–1511

Smull, B., Bousquet, O. and Steiner, M. 2000 'Contrasting stratification and mesoscale airflow in two heavy precipitation events observed during MAP'. Pp. 15–18 in Preprints of the 9th Conference on mountain meteorology, Aspen, Colorado. American Meteorological Society, Boston, USA

Srivastava, R. C. 1987 A model of intense downdrafts driven by the melting and evaporation of precipitation. *J. Atmos. Sci.*, **44,** 1752–1773

Srivastava, R. C., Matejka, T. J. and Lorello, T. J. 1986 Doppler radar study of the trailing anvil region associated with a squall line. *J. Atmos. Sci.*, **43,** 356–377

Steinacker, R. 1984 Area–height distribution of a valley and its relation to the valley wind. *Contrib. Atmos. Phys.*, **57,** 64–71

Steiner, M., Smith, J. A., Smull, B. and Houze Jr, R. A. 2000 'Airflow within major river valleys on the south side of the Alps as observed during the MAP Special Observing Period'. Pp. 11–14 in Preprints of the 9th Conference on mountain meteorology, Aspen, Colorado. American Meteorological Society, Boston, USA

Steiner, M., Bousquet, O., Houze Jr, R. A. and Smull, B. F. 2002 'Airflow within major Alpine river valleys: The concept of wet drainage flow'. Pp. 157–160 in Preprints of the 10th Conference on mountain meteorology, Park City, Utah. American Meteorological Society, Boston, USA

Stewart, J. Q., Whiteman, C. D., Steenburgh, W. J. and Bian, X. 2002 A climatological study of thermally driven wind systems of the US Intermountain West. *Bull. Am. Meteorol. Soc.*, **83,** 699–708

Vergeiner, I. and Dreiseitl, E. 1987 Valley winds and slope winds—observations and elementary thoughts. *Meteorol. Atmos. Phys.*, **36,** 264–286

Whiteman, C. D. 1982 Breakup of temperature inversions in deep mountain valleys. Part I: Observations. *J. Appl. Meteorol.*, **21,** 270–289

1990 Observations of thermally developed wind systems in mountainous terrain. Pp. 5–42 in *Atmospheric processes over complex terrain*. Ed. W. Blumen. Meteorological Monographs, Vol. 23, No. 45, American Meteorological Society, Boston, USA

Whiteman, C. D. and Doran, J. C. 1993 The relationship between overlying synoptic-scale flows and winds within a valley. *J. Appl. Meteorol.*, **32,** 1669–1682

Wurman, J., Straka, J., Rasmussen, E., Randall, M. and Zahrai, A. 1997 Design and deployment of a portable, pencil-beam, pulsed, 3 cm Doppler radar. *J. Atmos. Oceanic Technol.*, **14,** 1502–1512

Zängl, G., Egger, J. and Wirth, V. 2001 Diurnal winds in the Himalayan Kali Gandaki valley. Part II: Modeling. *Mon. Weather Rev.*, **129,** 1062–1080

Zipser, E. J. 1969 The role of organized unsaturated convective downdrafts in the structure and rapid decay of an equatorial disturbance. *J. Appl. Meteorol.*, **8,** 799–814

1977 Mesoscale and convective-scale downdrafts as distinct components of squall-line circulation. *Mon. Weather Rev.*, **105,** 1568–1589